Original Article

Multiparameter computed tomography (CT) radiomics signature fusion-based model for the preoperative prediction of clear cell renal cell carcinoma nuclear grade: a multicenter development and external validation study

Yingjie Xv[1#], Zongjie Wei[1#], Fajin Lv[2], Qing Jiang[3], Haoming Guo[2], Yineng Zheng[2], Xuan Zhang[4], Mingzhao Xiao[1]

[1]Department of Urology, The First Affiliated Hospital of Chongqing Medical University, Chongqing, China; [2]Department of Radiology, The First Affiliated Hospital of Chongqing Medical University, Chongqing, China; [3]Department of Urology, The Second Affiliated Hospital of Chongqing Medical University, Chongqing, China; [4]Department of Urology, Yongchuan Hospital of Chongqing Medical University, Chongqing, China

Contributions: (I) Conception and design: M Xiao, X Zhang, Y Xv; (II) Administrative support: M Xiao, Y Xv; (III) Provision of study materials or patients: Y Xv, X Zhang, Q Jiang, H Guo; (IV) Collection and assembly of data: Y Xv, Z Wei, Q Jiang, H Guo; (V) Data analysis and interpretation: Y Xv, Z Wei; (VI) Manuscript writing: All authors; (VII) Final approval of manuscript: All authors.

[#]These authors contributed equally to this work.

Correspondence to: Mingzhao Xiao, MD. Department of Urology, The First Affiliated Hospital of Chongqing Medical University, No. 1 Youyi Road, Yuzhong, Chongqing 400016, China. Email: mingzhaoxiao@cqmu.edu.cn; Xuan Zhang, MD. Department of Urology, Yongchuan Hospital of Chongqing Medical University, No. 439 Xuanhua Road, Yongchuan, Chongqing 402160, China. Email: xuanzhang168@163.com; Yineng Zheng, PhD. Department of Radiology, The First Affiliated Hospital of Chongqing Medical University, No. 1 Youyi Road, Yuzhong, Chongqing 400016, China. Email: yinengzheng@cqmu.edu.cn.

Background: The preoperative prediction of the pathological nuclear grade of clear cell renal cell carcinoma (CCRCC) is crucial for clinical decision making. However, radiomics features from one or two computed tomography (CT) phases are required to predict the CCRCC grade, which reduces the predictive performance and generalizability of this method. We aimed to develop and externally validate a multiparameter CT radiomics-based model for predicting the World Health Organization/International Society of Urological Pathology (WHO/ISUP) grade of CCRCC.

Methods: A total of 500 CCRCC patients at The First, Second, and Yongchuan Hospitals of Chongqing Medical University between January 2016 and May 2022 were retrospectively enrolled in this study. The patients were divided into the training set (n=268), internal testing set (n=115), and two external testing sets (testing set 1, n=62; testing set 2, n=55). Radiomics features were extracted from multi-phase CT images, and radiomics signatures (RSs) were created by least absolute shrinkage and selection operator (LASSO) regression. In addition, a clinical model was developed. A combined model was also established that integrated the RSs with the clinical factors, and was visualized via a nomogram. The performance of the established model was assessed using area under the curve (AUC) values, a calibration curve analysis, and a decision curve analysis (DCA).

Results: Among the four RSs and the clinical model, the RS-Triphasic had the best predictive performance with AUCs of 0.88 [95% confidence interval (CI): 0.85–0.91] and 0.84 (95% CI: 0.74–0.95) in the training and testing sets, respectively, and 0.82 (95% CI: 0.72–0.93) and 0.82 (95% CI: 0.71–0.93) in external testing sets 1 and 2. Integrating the RS-Triphasic, RS-corticomedullary phase (CMP), RS-nephrographic phase (NP), RS-non-contrast phase (NCP) with the clinical risk factors, a combined model was established with AUCs of 0.92 (95% CI: 0.89–0.94), 0.86 (95% CI: 0.76–0.95), 0.84 (95% CI: 0.73–0.95), and 0.82 (95% CI: 0.70–0.94)

for the training, internal testing, and external testing sets 1 and 2, respectively. The DCA indicated that the nomogram had a greater overall net benefit than the clinical and radiomics models.

Conclusions: The multiparameter CT RS fusion-based model had high accuracy in differentiating between high- and low-grade CCRCC preoperatively. Thus, it has great potential as a useful tool for personalized treatment planning and clinical decision making for CCRCC patients.

Keywords: Computed tomography (CT); radiomics; clear cell renal cell carcinoma (CCRCC); pathological nuclear grade; multiparameter fusion radiomics model

Submitted Jan 07, 2024. Accepted for publication Aug 01, 2024. Published online Sep 12, 2024.
doi: 10.21037/qims-24-35
View this article at: https://dx.doi.org/10.21037/qims-24-35

Introduction

Renal cell carcinoma (RCC) is the sixth and tenth most commonly diagnosed cancer among men and women worldwide, respectively (1,2). Over 70% of RCC cases are clear cell renal cell carcinoma (CCRCC), which contributes to the majority of fatalities among RCC patients (3). The pathological nuclear grade is a key prognostic factor for CCRCC. High-grade (grades III and IV) patients tend to have a lower five-year survival rate and overall survival time than those with low-grade (grades I and II) CCRCC (4-6). Additionally, the heterogeneity in tumor progression between high- and low-grade CCRCC affects the available treatment options (7). Currently, the only way to determine the nuclear grade is through biopsy, which is invasive and labor intensive. Thus, there is a pressing need for non-invasive, accurate, and labor-free tools to predict the grading level of CCRCC preoperatively.

Two systems have been used to estimate the nuclear grade of CCRCC: the Fuhrman grading system, and the 2016 World Health Organization/International Society of Urological Pathology (WHO/ISUP) system (8). Recently, the use of the WHO/ISUP system in practice has surpassed that of the Fuhrman grading system due to its advantages in applicability, repeatability, and clinical interrelation (8-10). The preoperative prediction of WHO/ISUP grades for CCRCC patients has more clinical management benefits than the Fuhrman grading system.

Computed tomography (CT) is the most common diagnostic tool for patients with CCRCC, due to its ability to stage tumors and evaluate invasiveness (11,12). However, the ability of CT to predict the nuclear grades of CCRCC is unsatisfactory, as the accuracy of CT image-based assessments depends on the subjective judgments of radiologists, which are empirically and manually dependent, and have low repeatability (13,14).

A radiomics approach enables high-throughput feature extraction from medical images, transforming imaging data into high-resolution mining data that reveals the spatial and temporal heterogeneity of tumors (15,16). Several studies have shown that CT image-based radiomics methods can assist in assessing the clinical progression of multiple cancers, including CCRCC, by differentiating between benign and malignant tumors, predicting the pathological subtypes of neoplasms and patient prognosis, and so on (14,17-24). However, most previous studies have largely relied on radiomics features from one or two CT phases to predict the CCRCC grade, and few have adopted more than one external set to validate their findings, resulting in reduced predictive performance and generalizability (21,25,26). To address this issue, this study sought to develop a multiparameter CT radiomics-based model that combines three-phase CT-rooted radiomics signatures (RSs) with clinical parameters to preoperatively predict the WHO/ISUP grades of CCRCC, and validate our findings using two external datasets. We present this article in accordance with the TRIPOD reporting checklist (27,28) (available at https://qims.amegroups.com/article/view/10.21037/qims-24-35/rc).

Methods

Study cohorts

The study was conducted in accordance with the Declaration of Helsinki (as revised in 2013). This retrospective study was approved by the Institutional Ethics Review Board of The First Affiliated Hospital of Chongqing Medical University (approval number: 2022-KY508), and the requirement of informed consent was

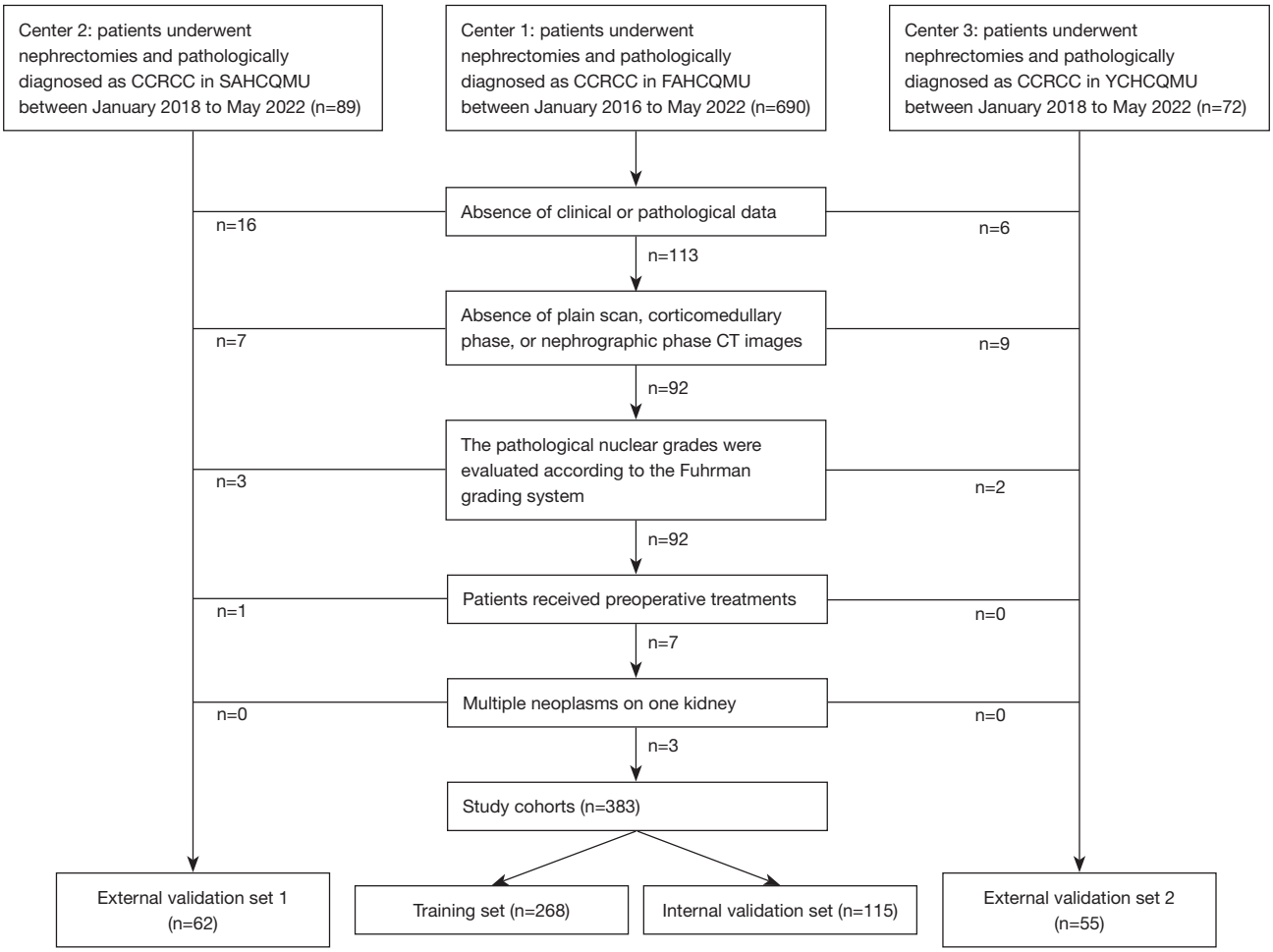

Figure 1 Flowchart of patient recruitment. Center 1 (FAHCQMU), The First Affiliated Hospital of Chongqing Medical University; Center 2 (SAHCQMU), The Second Affiliated Hospital of Chongqing Medical University; Center 3 (YCHCQMU), Yongchuan Hospital of Chongqing Medical University; CCRCC, clear cell renal cell carcinoma; CT, computed tomography.

waived due to the retrospective nature of this multicenter study. All the participating hospitals were informed of and agreed to participate in the study.

Patients who underwent nephrectomies at The First Affiliated Hospital of Chongqing Medical University (FAHCQMU) between January 2016 to May 2022 and had a pathologically confirmed diagnosis of CCRCC were recruited for the study. A total of 690 patients were enrolled in the study. Patients were excluded from the study if they met any of the following exclusion criteria: (I) had incomplete clinical or pathological data (n=113); (II) had their pathological nuclear grade evaluated according to the Fuhrman grading system (n=92); (III) had incomplete clear plain scan, corticomedullary phase (CMP), or nephrographic phase (NP) CT images (n=92); (IV) had undergone preoperative therapies (n=7); and/or (V) had multiple tumors on one kidney (n=3). It should be noted that the patients with multiple tumors on one kidney were excluded to ensure the internal and external validity of our study. Ultimately, 383 patients were included in this study. These patients were randomly divided into the training (n=268) and internal testing (n=115) sets at a ratio of 7:3. Patients from The Second Affiliated Hospital of Chongqing Medical University and Yongchuan Hospital of Chongqing Medical University were recruited between January 2018 to May 2022 using the same inclusion and exclusion criteria set out above, and were included as the external testing set 1 (n=62) and the external testing set 2 (n=55). The patient enrolment flowchart is shown in *Figure 1*.

Clinical variables, such as age, sex, tumor size (which

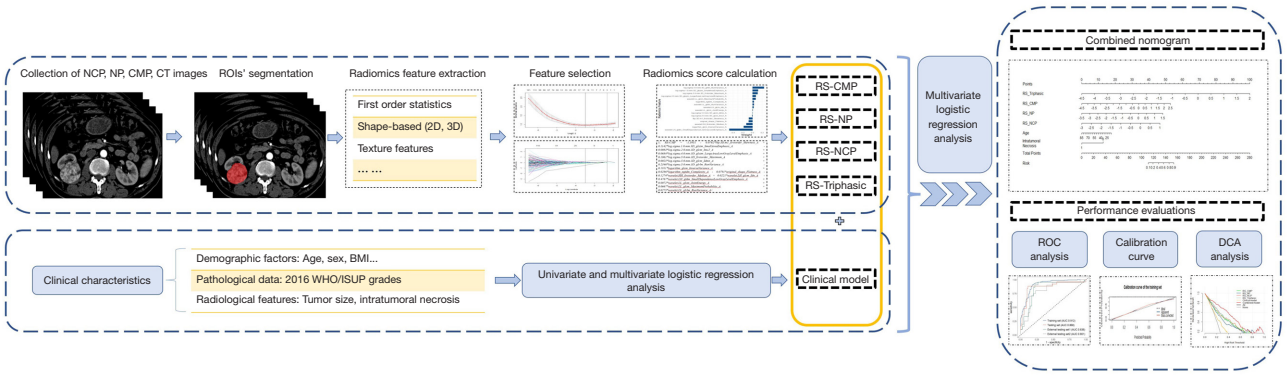

Figure 2 The overall workflow of the feature selection and model building procedures. NCP, non-contrast phase; NP, nephrographic phase; CMP, corticomedullary phase; CT, computed tomography; ROIs, regions of interest; 2D, two-dimensional; 3D, three-dimensional; RS, radiomics signature; BMI, body mass index; WHO/ISUP, World Health Organization/International Society of Urological Pathology; ROC, receiver operator characteristic; DCA, decision curve analysis.

was defined as the maximum diameter of the tumor), intratumoral necrosis [which was defined as the non-enhancement regions within the tumor during both the corticomedullary and NPs (29)], body mass index (BMI), clinical tumor-node-metastasis (TNM) stage [according to the standard TNM criteria, which were developed jointly by the Union for International Cancer Control and American Joint Committee on Cancer (30)], and the WHO/ISUP grades, were collected from the respective institutional electronic medical record systems of the hospitals. Under the two-tiered CCRCC classification system used in this study, grades I and II were designated as low-grade tumors, and grades III and IV as high-grade tumors. Previous research has shown that this system provides comparable survival information to the WHO/ISUP grading system (31).

CT examinations

Contrast-enhanced CT examinations were conducted within two weeks before the nephrectomy operations. The CT acquisition parameters are set out in Table S1. Iodinated nonionic contrast agent (dose: 1 mL/kg of body weight) was administered via an electric power injector into the antecubital vein at a rate of 2.5–3.0 mL/s. A non-contrast phase (NCP) CT scan of the abdomen was performed, followed by three post-contrast CT scans acquired at different phases; that is, the CMP, which was obtained 30 seconds after contrast administration; the NP, which was acquired 80 seconds after contrast administration; and the excretory phase (EP), which was obtained 180 seconds after contrast administration. Two independent radiologists (both with 10 years of experience in assessing abdominal and urological CT images) reported the radiological features, such as intratumoral necrosis and tumor size, based on the contrast-enhanced CT images, and any discrepancies were re-evaluated by a third senior radiologist (with over 20 years of experience in evaluating abdominal and urological CT images). As a large number of the patients lacked EP images, only NPC, CMP, and NP images were downloaded in Digital Imaging and Communications in Medicine format, and selected for the subsequent radiomics analysis. The overall workflow for the feature selection and model building procedures are shown in *Figure 2*.

Segmentation of tumor regions and extraction of radiomics features

An independent radiologist (Reader 1, who had 5 years of experience in abdominal imaging diagnosis) manually segmented the tumor regions and delineated the regions of interest (ROIs) using ITK-SNAP software (version 3.8.0). The ROIs were first delineated on the CMP images, followed by the NP images, and then the NCP images. To evaluate the reproducibility radiomics features, 30 patients were randomly selected for ROI re-segmentation by Reader 1 and another radiologist (Reader 2, who had 5 years of experience in abdominal imaging diagnosis). Each patient's images from all three phases were included, resulting in a total of 90 images (30 images per phase). The intra-class and inter-class correlation coefficients were calculated. Features with both intra-class and inter-class correlation coefficients >0.80 were included in the subsequent analysis.

The CT images were re-sampled to a voxel of 1×1×1 mm^3 via B-spline interference, and underwent gray-level discretization. Next, using the "Pyradiomics" (32) package in Python (version 3.7.1), the radiomics features were extracted and separately standardized via z-scores. The mean and standard deviation (SD) of the training set were used to normalize the internal and external testing cohorts, resulting in standardized features to ensure an accurate and reliable analysis. The types of radiomics features extracted in this study are listed in Table S2.

To address the imbalance in patient numbers between the high-grade (n=59) and low-grade (n=209) CCRCCs, we applied the synthetic minority oversampling technique to the training set. This technique involved generating synthetic samples in the minority class to achieve a more balanced representation of the classes, improving the model's performance in predicting high-grade CCRCCs that were underrepresented in the data (33).

Selection of radiomics features

First, a *t*-test was performed to identify significant differences in radiomics features between the low- and high-grade CCRCCs in the training cohort. Next, these features were processed by five-fold cross-validation least absolute shrinkage and selection operator (LASSO) regression to identify the subset of features with the best predictive ability for distinguishing between high- and low-grade CCRCC. Radiomics scores were calculated according to the weight coefficients of the features selected by LASSO regression, and four RSs; that is, RS-Triphasic, RS-CMP, RS-NP, and RS-NCP, were established.

Model construction

The RS-Triphasic, RS-CMP, RS-NP, RS-NCP, and clinical variables were integrated, and multivariate logistic and forward-backward stepwise regression analyses were conducted. A final reduced multivariate logistic regression analysis was conducted to identify the factors that could predict high-grade CCRCC, and a combined model was constructed and visualized via a user-friendly nomogram. Employing clinical parameters only, a clinical model was built using the same method described above.

Performance evaluation

The predictive performance of the established models was evaluated via a receiver operating characteristic (ROC) curve analysis using the area under the curve (AUC) values. The accuracy, sensitivity, specificity, positive predictive value, and negative predictive value were determined using the cut-off values. To assess the discrimination ability of the radiomics nomogram, calibration curves were created using bootstrapping with 1,000 re-samples. The clinical utility of the established models was evaluated by decision curve analysis (DCA).

Quality control

This study followed the guidelines provided by the Image Biomarker Standardization Initiative to ensure standardization (34). Additionally, the reliability of the research was assessed using the radiomics quality score (RQS; version 1.0) (35). The RQS for this study was 19, which represents a score of 52.8%. Detailed information on the scoring can be found in Appendix 1.

Statistical analysis

The normality of the continuous variables was evaluated using the Shapiro-Wilk test. The normally distributed continuous variables are reported as the mean (SD), and were compared using the Student's *t*-test. The categorical variables were compared using the chi-square or Fisher's exact test. All the data analyses were conducted using R software (version 4.1.2) and SPSS software (version 23.0). A two-tailed P value <0.05 was considered statistically significant.

Results

Clinical characteristics

A total of 500 patients (male to female ratio: 298:202; low- to high-grade ratio: 373:127; average age: 57.86±11.95 years) who met the inclusion and exclusion criteria were included in this study. Among them, 383 patients were recruited from the FAHCQMU and divided into a training set (n=268) and an internal testing set (n=115), while the remaining patients were assigned to external testing sets 1 (n=62) and 2 (n=55). *Table 1* provides a summary of the baseline clinical characteristics of the whole study cohort.

The differences in the clinical variables between the patients with low- and high-grade CCRCCs are summarized in *Table 2* for the training, internal, and

Table 1 Baseline clinical characteristics of the whole study cohort

Variables	All patients (n=500)
Pathological nuclear grade, n (%)	
Low	373 (74.6)
High	127 (25.4)
Age (years), mean ± SD	57.86±11.95
Sex, n (%)	
Male	298 (59.6)
Female	202 (40.4)
BMI (kg/m^2), mean ± SD	24.24±3.91
Tumor size (cm), mean ± SD	4.56±2.33
Intratumoral necrosis, n (%)	192 (38.4)
Clinical T stage ≥2, n (%)	55 (11.0)
Clinical N stage 1, n (%)	14 (2.8)
Clinical M stage 1, n (%)	6 (1.2)

n, number; SD, standard deviation; BMI, body mass index.

external validation sets. In the training cohort, patients with high-grade CCRCCs had larger tumor sizes (P<0.0001), a higher incidence of intratumoral necrosis (P<0.0001), and were at higher clinical T (P<0.0001), N (P<0.0001), and M (P=0.001) stages than the low-grade CCRCC patients.

Selection of radiomics features

A total of 1,743 radiomics features were extracted from the CT images of each phase (i.e., CMP, NP, and NCP). A total of 1,312 features extracted from the CMP with both the inter- and intra-observer correlation coefficients >0.80 were fed into the *t*-test and LASSO algorithm, and 16 features were found to have a superior discriminatory ability to assess nuclear grade (*Figure 3A*,*3B*). The weighting coefficients of the selected features are shown in *Figure 3C*. Similar selection methods were applied to the NP and NCP radiomics features, leading to the identification of 14 and 11 selected features, respectively (*Figure 3D-3I*).

The radiomics features from the three phases were combined. Of the 3,519 features that exhibited good repeatability, the *t*-test analysis and LASSO screening resulted in 25 features, comprising 9 features from the CMP images, 4 from the NP images, and 12 from the NCP images (*Figure 3J-3L*). The correlation heatmaps of the selected radiomics features are shown in Figures S1-S4.

Table 2 Comparison of clinical factors between low- and high-grade CCRCCs in the training, internal testing, and external testing sets

Clinical variables	Training set (n=268)			Internal testing set (n=115)			External testing set 1 (n=62)			External testing set 2 (n=55)		
	Low-grade (n=208)	High-grade (n=60)	P	Low-grade (n=90)	High-grade (n=25)	P	Low-grade (n=41)	High-grade (n=21)	P	Low-grade (n=34)	High-grade (n=21)	P
Age (year), mean ± SD	57.45±12.54	56.93±11.84	0.78	56.93±11.13	54.96±12.50	0.45	60.22±10.75	65.86±10.68	0.06	57.18±11.16	60.38±11.25	0.31
Sex, n (%)			0.08			0.027			0.13			0.77
Male	119 (57.2)	42 (70.0)		50 (55.6)	20 (80)		22 (53.7)	14 (66.7)		23 (67.6)	15 (71.4)	
Female	89 (42.8)	18 (30.0)		40 (44.4)	5 (20)		19 (46.3)	7 (33.3)		11 (32.4)	6 (28.6)	
BMI (kg/m^2), mean ± SD	24.46±4.03	23.49±2.80	0.08	24.32±5.01	23.42±3.86	0.41	25.20±2.94	24.84±2.22	0.63	24.40±3.64	22.06±2.37	0.01
Tumor size (cm), mean ± SD	4.24±2.08	6.01±3.24	<0.0001	3.81±1.43	6.21±2.18	<0.0001	3.83±1.46	6.48±2.00	<0.0001	4.43±2.67	4.50±2.63	0.93
Intratumoral necrosis, n (%)	79 (38.0)	40 (66.7)	<0.0001	32 (35.6)	16 (64.0)	0.011	3 (7.3)	13 (61.9)	<0.0001	6 (17.6)	3 (14.3)	0.74
Clinical T stage ≥ 2, n (%)	23 (11.1)	23 (38.3)	<0.0001	0 (0.0)	2 (8.0)	0.07	0 (0.0)	4 (19.0)	0.004	2 (5.9)	1 (4.8)	0.86
Clinical N stage 1, n (%)	2 (1.0)	6 (10.0)	<0.0001	0 (0.0)	2 (8.0)	0.007	0 (0.0)	3 (14.3)	0.013	0 (0.0)	1 (4.8)	0.20
Clinical M stage 1, n (%)	0 (0.0)	3 (5.0)	0.001	0 (0.0)	0 (0.0)	–	0 (0.0)	2 (9.5)	0.05	0 (0.0)	1 (4.8)	0.20

CCRCC, clear cell renal cell carcinoma; SD, standard deviation; BMI, body mass index.

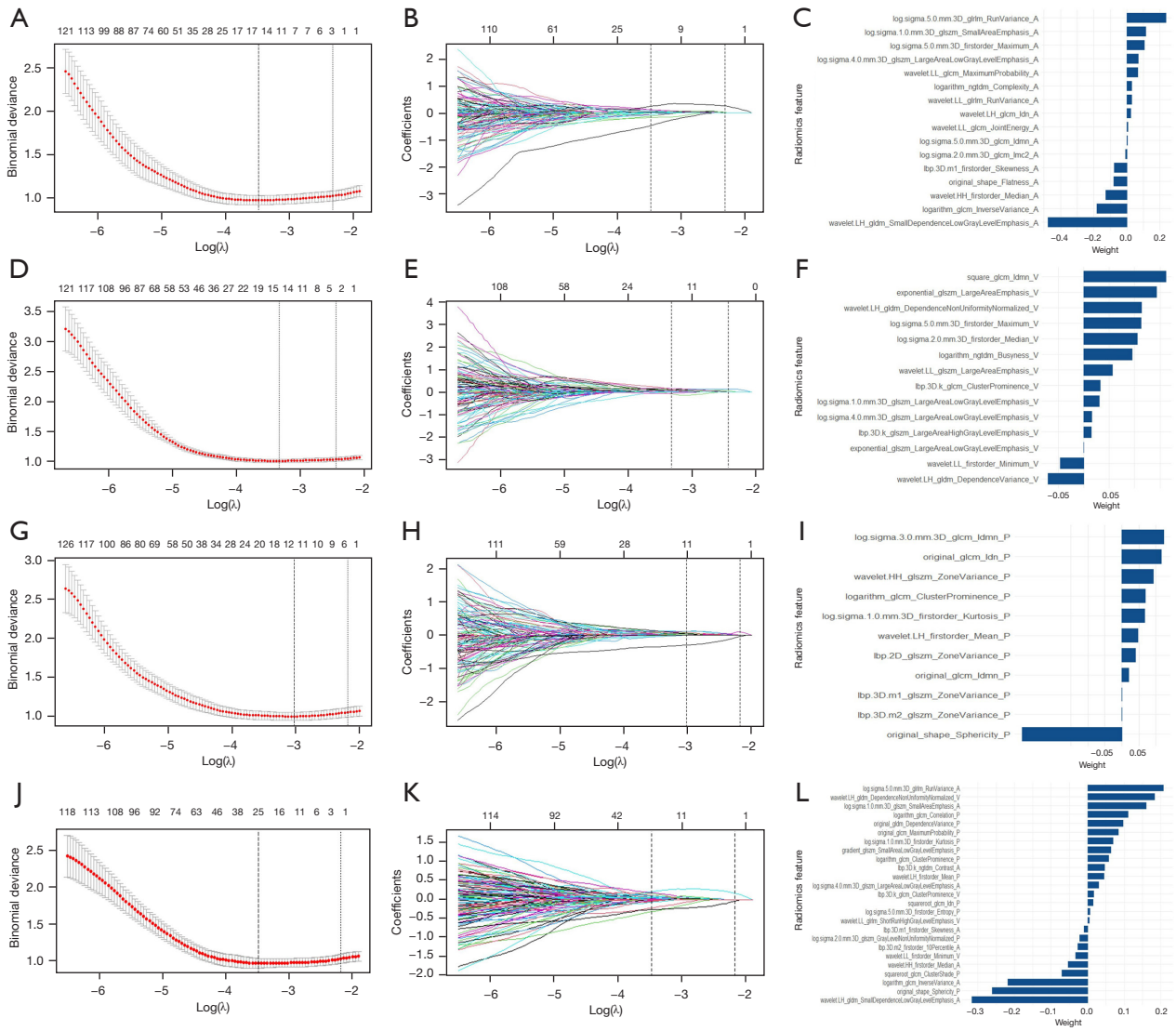

Figure 3 The radiomics feature selection results using the LASSO algorithm. Based on minimum criteria, LASSO regression selected 16, 14, 11, and 25 radiomics features from the (A) CMP, (D) NP, (G) NCP, and (J) Triphasic CT images, respectively, with Tuning parameter (λ) values of 0.0309, 0.0362, 0.0489, and 0.0309, respectively. The coefficient profile plots of the identified non-zero coefficients for (B) CMP, (E) NP, (H) NCP, and (K) Triphasic radiomics features were generated against the selected log λ values. The names and corresponding weighting coefficients of the selected (C) CMP, (F) NP, (I) NCP, and (L) Triphasic radiomics features. LASSO, least absolute shrinkage and selection operator; CMP, corticomedullary phase; NP, nephrographic phase; NCP, non-contrast phase; CT, computed tomography.

Radiomics model construction

Four RSs (i.e., RS-CMP, RS-NP, RS-NCP, and RS-Triphasic) were established according to the formulas detailed in Appendix 2. As *Table 3* shows, RS-Triphasic had the best predictive performance with AUCs of 0.88 [95% confidence interval (CI): 0.85–0.91] and 0.84 (95% CI: 0.74–0.95) in the training and internal testing set, respectively, and 0.82 (95% CI: 0.72–0.93) and 0.82 (95% CI: 0.71–0.93) in external testing sets 1 and 2 (*Figure 4A*), followed by RS-CMP with AUCs of 0.84 (95% CI: 0.81–0.88), 0.83 (95% CI: 0.71–0.95), 0.80 (95% CI: 0.68–0.91), and 0.80 (95% CI: 0.69–0.92) in the training, internal testing, and external testing sets 1 and 2, respectively (*Figure 4B*). RS-NP ranked third in terms of its performance, and RS-NCP was the worst-performing RS (*Figure 4C,4D*).

Table 3 Predictive performances of the established models in the training, internal testing, and external testing sets 1 and 2

Model	Study cohort	AUC (95% CI)	Accuracy	Sensitivity	Specificity	PPV	NPV
Combined model	Training	0.92 (0.89–0.94)	0.84	0.84	0.84	0.84	0.84
	Internal testing	0.86 (0.76–0.95)	0.84	0.64	0.90	0.64	0.90
	External testing 1	0.84 (0.73–0.95)	0.79	0.76	0.81	0.67	0.87
	External testing 2	0.82 (0.70–0.94)	0.73	0.91	0.62	0.59	0.91
RS-Triphasic	Training	0.88 (0.85–0.91)	0.80	0.76	0.83	0.82	0.78
	Internal testing	0.84 (0.74–0.95)	0.85	0.80	0.87	0.63	0.94
	External testing 1	0.82 (0.72–0.93)	0.77	0.67	0.83	0.67	0.83
	External testing 2	0.82 (0.71–0.93)	0.73	0.95	0.60	0.58	0.73
RS-CMP	Training	0.84 (0.81–0.88)	0.77	0.66	0.89	0.86	0.72
	Internal testing	0.83 (0.71–0.95)	0.81	0.80	0.81	0.54	0.94
	External testing 1	0.80 (0.68–0.91)	0.77	0.86	0.73	0.62	0.91
	External testing 2	0.80 (0.69–0.92)	0.67	1.00	0.49	0.53	1.00
RS-NP	Training	0.84 (0.80–0.88)	0.77	0.75	0.79	0.78	0.76
	Internal testing	0.82 (0.72–0.91)	0.79	0.68	0.82	0.52	0.90
	External testing 1	0.78 (0.66–0.90)	0.71	0.57	0.78	0.57	0.78
	External testing 2	0.78 (0.65–0.90)	0.71	0.75	0.69	0.58	0.83
RS-NCP	Training	0.83 (0.79–0.87)	0.76	0.65	0.88	0.84	0.71
	Internal testing	0.81 (0.72–0.91)	0.83	0.32	0.97	0.73	0.84
	External testing 1	0.79 (0.68–0.90)	0.73	0.52	0.83	0.61	0.77
	External testing 2	0.77 (0.63–0.91)	0.76	0.65	0.83	0.68	0.81
Clinical model	Training	0.76 (0.72–0.81)	0.69	0.62	0.76	0.72	0.67
	Internal testing	0.74 (0.62–0.87)	0.77	0.68	0.80	0.49	0.90
	External testing 1	0.73 (0.58–0.87)	0.68	0.71	0.66	0.52	0.82
	External testing 2	0.70 (0.54–0.85)	0.69	0.55	0.77	0.58	0.75

AUC, area under the curve; CI, confidential interval; PPV, positive prediction value; NPV, negative prediction value; RS, radiomics signature; CMP, corticomedullary phase; NP, nephrographic phase; NCP, non-contrast phase.

Clinical model building

Based on the results of the multivariate logistic regression analysis, age [odds ratio (OR): 0.98, 95% CI: 0.97–1.00], sex (OR: 0.68, 95% CI: 0.45–1.03), intratumoral necrosis (OR: 0.54, 95% CI: 0.33–0.88), and tumor size (OR: 1.40, 95% CI: 1.26–1.55) were included in the clinical model (Table S3). The clinical model had AUCs of 0.76 (95% CI: 0.72–0.81), 0.74 (95% CI: 0.62–0.87), 0.73 (95% CI: 0.58–0.87), and 0.70 (95% CI: 0.54–0.85) in the training, internal testing, and external testing sets 1 and 2, respectively (*Table 3*). The ROC curves of the clinical model for the four study sets are shown in Figure S5.

Establishment of the combined model

RS-Triphasic, RS-CMP, RS-NP, and RS-NCP were integrated with clinical factors, and the multivariate logistic regression analysis was conducted. RS-Triphasic (OR: 4.98, 95% CI: 3.08–8.06), RS-CMP (OR: 2.11, 95% CI: 1.07–4.14), RS-NP (OR: 2.74, 95% CI: 1.03–7.29), RS-NCP (OR: 3.59, 95% CI: 1.46–8.82), age (OR: 0.97, 95%

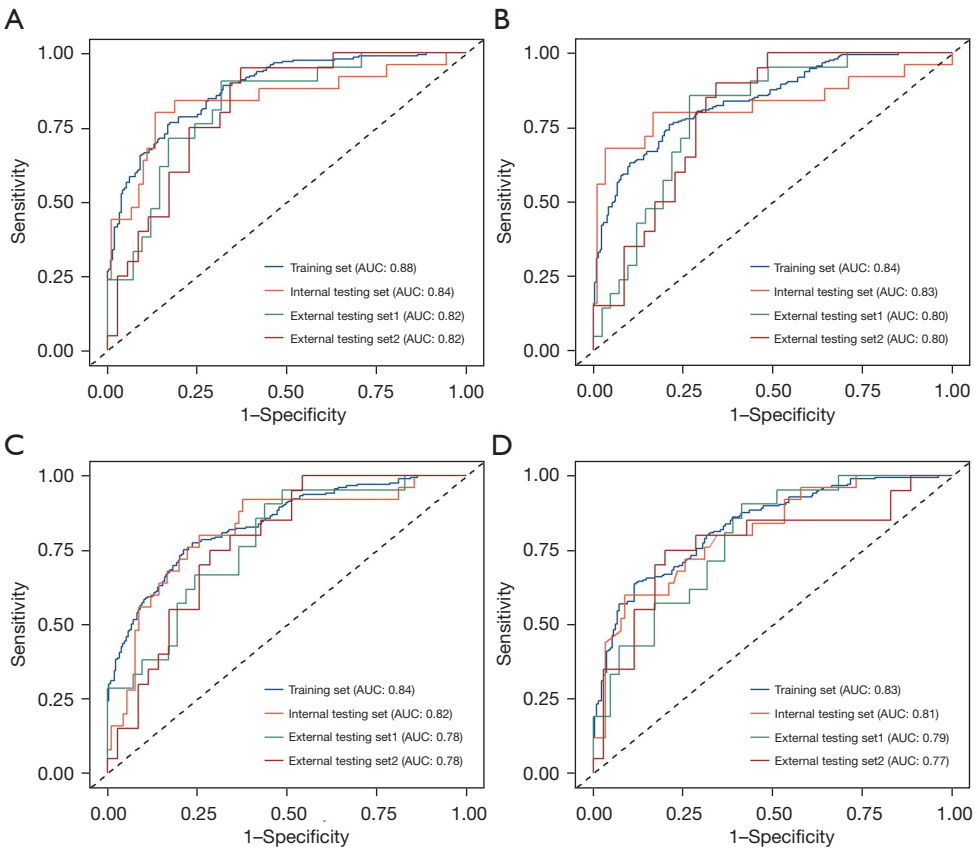

Figure 4 The ROC curves of the (A) RS-Triphasic, (B) RS-CMP, (C) RS-NP, and (D) RS-NCP in the training, internal testing, and external testing sets 1 and 2. AUC, area under the curve; ROC, receiver operator characteristic; RS, radiomics signature; CMP, corticomedullary phase; NP, nephrographic phase; NCP, non-contrast phase.

CI: 0.95–1.00), and intratumoral necrosis (OR: 0.26, 95% CI: 0.14–0.49) were found to be independent risk factors for patients with high-grade CCRCC (*Table 4*). A combined model was thus established with AUCs of 0.92 (95% CI: 0.89–0.94), 0.86 (95% CI: 0.76–0.95), 0.84 (95% CI: 0.73–0.95), and 0.82 (95% CI: 0.70–0.94) in the training, internal testing, and two external testing sets, respectively, with accuracies of 0.84, 0.79, and 0.73, and sensitivities of 0.64, 0.76, and 0.91 in the internal and two external testing sets, respectively (*Figure 5A,5B*). A user-friendly nomogram was plotted (*Figure 5A*). *Table 3* details the predictive performance of the nomogram in the four study cohorts.

In terms of predicting the pathological nuclear grades of CCRCC, the DCA results showed that the combined model performed better across most threshold probabilities than the clinical and radiomics models (*Figure 5C*). The calibration curves of the nomogram in the different study cohorts are presented in *Figure 5D-5G*.

Discussion

This study developed and externally validated four RSs for the preoperative prediction of WHO/ISUP grades based on the data of 500 patients from three independent centers. A combined model that incorporated the RSs with clinical features was also established. The combined model showed excellent predictive performance in both the training, internal testing and external testing sets, and outperformed the clinical model and RSs. Due to the large-scale and multicenter design of this study, the established multiparameter CT radiomics-based model is more reliable than other models and easily applicable to clinical settings. Our findings indicated that the contrast-enhanced CT image-based radiomics method can reveal the differences in the pathological nuclear grades of CCRCC and may aid in personalized treatment planning for patients with different WHO/ISUP grading levels.

Table 4 The results of the full and reduced multivariate logistic regression analyses for nomogram construction

Variate	Full multivariate model			Reduced multivariate model		
	Coefficient	OR (95% CI)	P value	Coefficient	OR (95% CI)	P value
(Intercept)	8.26	3,858.71 (187.25–79,518.20)	<0.0001	8.06	3,154.31 (352.56–28,221.56)	<0.0001
RS-Triphasic	1.48	4.38 (2.65–7.25)	<0.0001	1.61	4.98 (3.08–8.06)	<0.0001
RS-CMP	0.74	2.09 (1.06–4.13)	0.03	0.75	2.11 (1.07–4.14)	0.03
RS-NP	1.05	2.85 (1.06–7.67)	0.04	1.01	2.74 (1.03–7.29)	0.04
RS-NCP	1.27	3.57 (1.44–8.84)	0.01	1.28	3.59 (1.46–8.82)	0.01
Age	–0.03	0.97 (0.95–1.00)	0.04	–0.03	0.97 (0.95–1.00)	0.03
Sex	–0.39	0.68 (0.38–1.22)	0.19	–	–	–
BMI	–0.04	0.97 (0.88–1.05)	0.44	–	–	–
Intratumoral necrosis	–1.52	0.22 (0.11–0.44)	<0.0001	–1.35	0.26 (0.14–0.49)	<0.0001
Tumor size	0.15	1.16 (0.95–1.42)	0.16	–	–	–
Clinical T stage ≥2	–0.41	0.67 (0.21–2.12)	0.49	–	–	–
Clinical N 1 stage	–1.37	0.26 (0.001–68.12)	0.63	–	–	–
Clinical M 1 stage	14.53	–	0.99	–	–	–

OR, odds ratio; CI, confidential interval; RS, radiomics signature; CMP, corticomedullary phase; NP, nephrographic phase; NCP, non-contrast phase; BMI, body mass index.

Several studies have explored the potential of radiomics methods to predict the WHO/ISUP grades of CCRCC, and these methods have presented with AUCs ranging from 0.810–0.910 in the testing sets (26,36-39). Our model showed comparable predictive performance. Unlike most previous studies that have employed single-center cohorts and have had limited sample sizes, we recruited a large study cohort from three independent medical centers (n=500); thus, our established models are more reliable and easier to generalize. We also used multiparameter CT imaging based radiomics features to capture comprehensive tumor characteristics from different CT phases, and constructed a more accurate triphasic model (the RS-Triphasic) using a post-fusion method.

The RS-Triphasic showed the best predictive performance among the four RSs with AUCs of 0.88 (95% CI: 0.85–0.91) and 0.84 (95% CI: 0.74–0.95) in the training and testing sets, respectively, and 0.82 (95% CI: 0.72–0.93) and 0.82 (95% CI: 0.71–0.93) in external testing sets 1 and 2. To further improve the predictive performance of the radiomics model, we also incorporated clinical factors. The results of the multivariate logistic regression analysis indicated that age (OR: 0.97, 95% CI: 0.95–1.00), intratumoral necrosis (OR: 0.26, 95% CI: 0.14–0.49), RS-Triphasic (OR: 4.98, 95% CI: 3.08–8.06), RS-CMP (OR: 2.11, 95% CI: 1.07–4.14), RS-NP (OR: 2.74, 95% CI: 1.03–7.29), and RS-NCP (OR: 3.59, 95% CI: 1.46–8.82) were independent diagnostic factors for high-grade CCRCC. A combined model was then built including these factors. The combined model had AUC values of 0.92 (95% CI: 0.90–0.94), 0.86 (95% CI: 0.76–0.95), 0.84 (95% CI: 0.73–0.95), and 0.82 (95% CI: 0.70–0.94) in the training, internal testing, and two external testing sets, respectively.

It should be noted that, age has been found to be a risk factor for high-grade CCRCC in previous studies (40); however, the results of the current study contradict this finding. The OR value for age was 0.97, which suggests that the promotability of this factor is very weak. The inconsistencies in these results may be due to selection bias. Moreover, while significant differences in tumor size distributions across the datasets were found, these discrepancies did not significantly affect our results. This is primarily because tumor size was excluded from the combined model for subgroup differentiation following the multivariate logistic regression analysis.

Additionally, while the RS-Triphasic included radiomics features from three CT imaging phases, its integration with individual RSs in the combined model served several critical

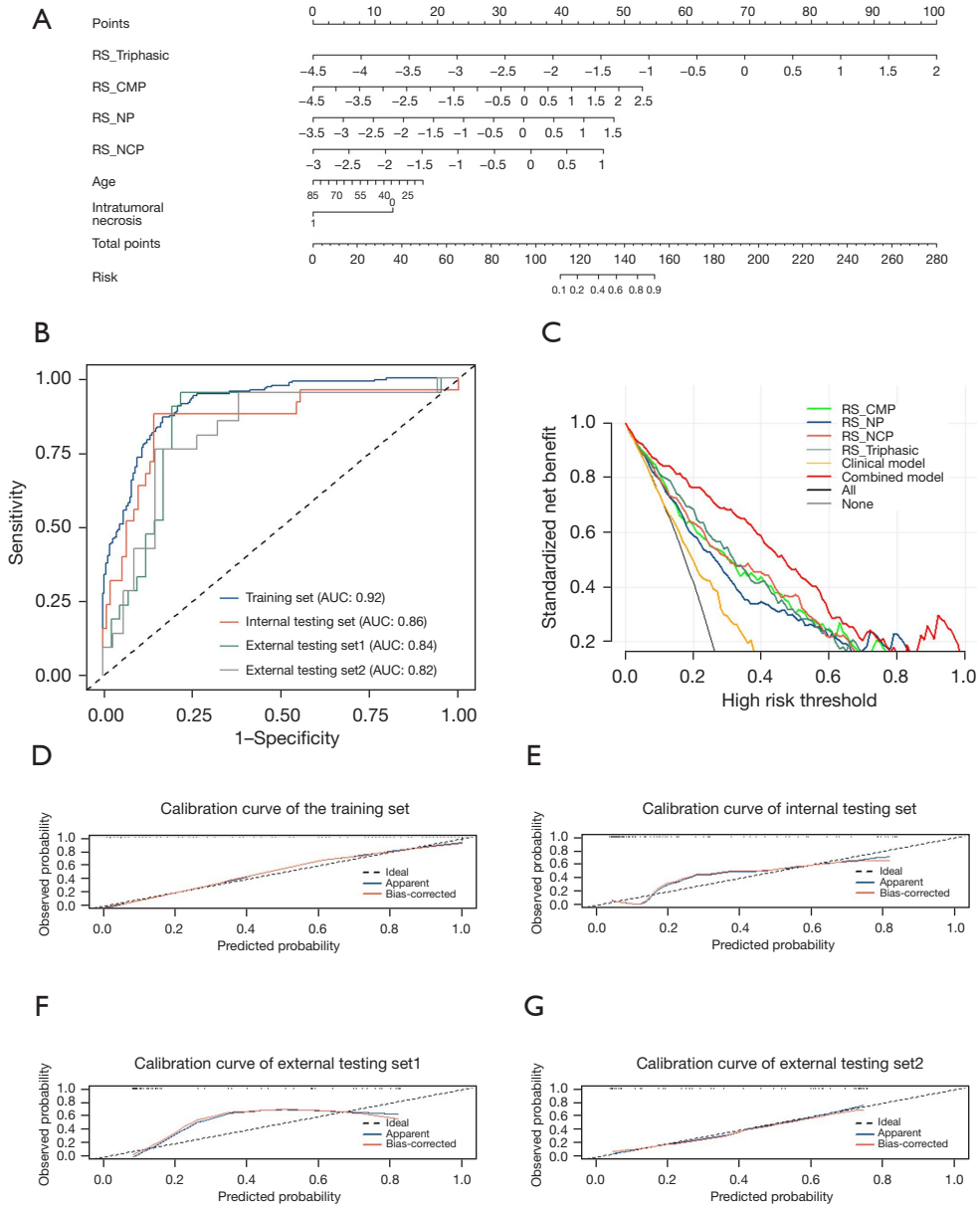

Figure 5 The establishment and performance evaluation of the nomogram. (A) The multivariate logistic regression indicated that RS-Triphasic, RS-CMP, RS-NP, RS-NCP, age, and intratumoral necrosis were independent risk factors for patients with high-grade CCRCC. A combined model was then constructed and visualized via a nomogram. (B) The ROC analysis of the combined model. (C) The DCA result showed that the combined model provides more benefits to patients with CCRCC across most thresholds. The calibration curve analysis of the combined model in the (D) training, (E) internal testing, and external testing sets (F) 1 and (G) 2. AUC, area under the curve; RS, radiomics signature; CMP, corticomedullary phase; NP, nephrographic phase; NCP, non-contrast phase; CCRCC, clear cell renal cell carcinoma; ROC, receiver operator characteristic; DCA, decision curve analysis.

purposes. First, variations in feature selection between the RS-Triphasic and individual RSs arose from differences in statistical properties and contributions to the predictive model. Second, the inclusion of the RS-Triphasic alongside the individual RSs captured a comprehensive range of radiomics features associated with CCRCC pathology, enhancing predictive accuracy. Additionally, this integration ensured a robust assessment of CCRCC pathology, considering potential variations in feature importance across imaging phases. Overall, the current study represents a significant advancement in the field of radiomics-based prediction of CCRCC grade. The multicenter design, the use of a multi-phase CT imaging protocol, and the incorporation of clinical factors all contribute to the increased accuracy and clinical utility of the predictive model.

This multiparameter CT RS fusion-based model has several advantages over traditional diagnostic tools, such as CT and percutaneous needle renal biopsy. One significant advantage of the radiomics model is its non-invasive nature; it does not require an invasive procedure like biopsy, which can be associated with a risk of complications, such as bleeding or infection (41-43). Moreover, the accurate grading of CCRCC can provide information about the aggressiveness of the cancer, and can aid in determining the optimal treatment strategy for each patient. For example, patients with low-grade CCRCC may be candidates for active surveillance or partial nephrectomy, while patients with high-grade CCRCC may require more aggressive treatments, such as radical nephrectomy or systemic therapy (44). The accurate preoperative prediction of CCRCC grades can also help clinicians determine the extent of surgery needed and guide the choice of the surgical approach (44,45). In addition, the nomogram can improve the accuracy of preoperative diagnosis and reduce the risk of underestimating the grade of CCRCC. CT or percutaneous needle renal biopsy can be limited by sampling errors or tumor heterogeneity, which can result in an inaccurate diagnosis (13). Conversely, the combined model uses radiomics features derived from multi-phase CT images and thus provides a more comprehensive assessment of tumor characteristics.

This study had several limitations. First, this study was retrospective; thus, selection bias is inevitable, and prospective validation is needed to confirm the generalizability of the findings. Second, the study focused on the preoperative prediction of CCRCC grade and did not evaluate the prognostic value of the radiomics-based model in predicting patient outcomes, such as survival or recurrence. Third, the study only included patients with CCRCC; thus, the performance of the radiomics-based nomogram in other types of RCC needs to be evaluated.

Conclusions

This study developed and externally validated a multi-phase CT radiomics-based model for the preoperative prediction of WHO/ISUP grades of CCRCC. This combined model integrated RSs with clinical factors, and showed high accuracy and outperformed clinical model and radiomics models alone. Thus, it may provide a more comprehensive approach for predicting the WHO/ISUP grade of CCRCC and may assist in the development of clinical and management strategies.

Acknowledgments

The authors would like to thank all the clinicians and technicians at the Radiology, Urology, and Pathology Departments at The First Affiliated Hospital of Chongqing Medical University who provided us with professional advice and guidance.

Funding: This research was supported by the Chongqing Talents and Famous Teachers Project (No. CQYC202003) and the Chongqing Municipal Education Commission's 14th Five-Year Key Discipline Support Project (No. 20240101).

Footnote

Reporting Checklist: The authors have completed the TRIPOD reporting checklist. Available at https://qims.amegroups.com/article/view/10.21037/qims-24-35/rc

Conflicts of Interest: All authors have completed the ICMJE uniform disclosure form (available at https://qims.amegroups.com/article/view/10.21037/qims-24-35/coif). The authors have no conflicts of interest to declare.

Ethical Statement: The authors are accountable for all aspects of the work in ensuring that questions related to the accuracy or integrity of any part of the work are appropriately investigated and resolved. The study was conducted in accordance with the Declaration of Helsinki (as revised in 2013). This study was approved by the Institutional Ethics Review Board of The First Affiliated

Hospital of Chongqing Medical University (approval number: 2022-KY508), and the requirement of informed consent was waived due to the retrospective nature of this multicenter study. All the participating hospitals were informed of and agreed to participate in the study.

References

1. Bukavina L, Bensalah K, Bray F, Carlo M, Challacombe B, Karam JA, Kassouf W, Mitchell T, Montironi R, O'Brien T, Panebianco V, Scelo G, Shuch B, van Poppel H, Blosser CD, Psutka SP. Epidemiology of Renal Cell Carcinoma: 2022 Update. Eur Urol 2022;82:529-42.
2. Capitanio U, Bensalah K, Bex A, Boorjian SA, Bray F, Coleman J, Gore JL, Sun M, Wood C, Russo P. Epidemiology of Renal Cell Carcinoma. Eur Urol 2019;75:74-84.
3. Hsieh JJ, Purdue MP, Signoretti S, Swanton C, Albiges L, Schmidinger M, Heng DY, Larkin J, Ficarra V. Renal cell carcinoma. Nat Rev Dis Primers 2017;3:17009.
4. Warren AY, Harrison D. WHO/ISUP classification, grading and pathological staging of renal cell carcinoma: standards and controversies. World J Urol 2018;36:1913-26.
5. Paner GP, Stadler WM, Hansel DE, Montironi R, Lin DW, Amin MB. Updates in the Eighth Edition of the Tumor-Node-Metastasis Staging Classification for Urologic Cancers. Eur Urol 2018;73:560-9.
6. Fuhrman SA, Lasky LC, Limas C. Prognostic significance of morphologic parameters in renal cell carcinoma. Am J Surg Pathol 1982;6:655-63.
7. Atkins MB, Tannir NM. Current and emerging therapies for first-line treatment of metastatic clear cell renal cell carcinoma. Cancer Treat Rev 2018;70:127-37.
8. Delahunt B, Eble JN, Egevad L, Samaratunga H. Grading of renal cell carcinoma. Histopathology 2019;74:4-17.
9. Browning L, Colling R, Verrill C. WHO/ISUP grading of clear cell renal cell carcinoma and papillary renal cell carcinoma; validation of grading on the digital pathology platform and perspectives on reproducibility of grade. Diagn Pathol 2021;16:75.
10. Delahunt B, Sika-Paotonu D, Bethwaite PB, William Jordan T, Magi-Galluzzi C, Zhou M, Samaratunga H, Srigley JR. Grading of clear cell renal cell carcinoma should be based on nucleolar prominence. Am J Surg Pathol 2011;35:1134-9.
11. Trevisani F, Floris M, Minnei R, Cinque A. Renal Oncocytoma: The Diagnostic Challenge to Unmask the Double of Renal Cancer. Int J Mol Sci 2022;23:2603.
12. Krishna S, Murray CA, McInnes MD, Chatelain R, Siddaiah M, Al-Dandan O, Narayanasamy S, Schieda N. CT imaging of solid renal masses: pitfalls and solutions. Clin Radiol 2017;72:708-21.
13. Gao Y, Zhao X, Wang X, Zhu C, Li C, Li J, Wu X. A Clinical Radiomics Nomogram Was Developed by Integrating Radiomics Signatures and Clinical Variables to Distinguish High-Grade ccRCC from Type 2 pRCC. J Oncol 2022;2022:6844349.
14. Demirjian NL, Varghese BA, Cen SY, Hwang DH, Aron M, Siddiqui I, Fields BKK, Lei X, Yap FY, Rivas M, Reddy SS, Zahoor H, Liu DH, Desai M, Rhie SK, Gill IS, Duddalwar V. CT-based radiomics stratification of tumor grade and TNM stage of clear cell renal cell carcinoma. Eur Radiol 2022;32:2552-63.
15. Mayerhoefer ME, Materka A, Langs G, Häggström I, Szczypiński P, Gibbs P, Cook G. Introduction to Radiomics. J Nucl Med 2020;61:488-95.
16. van Timmeren JE, Cester D, Tanadini-Lang S, Alkadhi H, Baessler B. Radiomics in medical imaging-"how-to" guide and critical reflection. Insights Imaging 2020;11:91.
17. Tong H, Sun J, Fang J, Zhang M, Liu H, Xia R, Zhou W, Liu K, Chen X. A Machine Learning Model Based on PET/CT Radiomics and Clinical Characteristics Predicts Tumor Immune Profiles in Non-Small Cell Lung Cancer: A Retrospective Multicohort Study. Front Immunol 2022;13:859323.
18. Perez-Johnston R, Araujo-Filho JA, Connolly JG, Caso R, Whiting K, Tan KS, Zhou J, Gibbs P, Rekhtman N, Ginsberg MS, Jones DR. CT-based Radiogenomic Analysis of Clinical Stage I Lung Adenocarcinoma with Histopathologic Features and Oncologic Outcomes. Radiology 2022;303:664-72.
19. Sun W, Liu S, Guo J, Liu S, Hao D, Hou F, Wang H, Xu W. A CT-based radiomics nomogram for distinguishing between benign and malignant bone tumours. Cancer Imaging 2021;21:20.
20. Xu X, Zhang HL, Liu QP, Sun SW, Zhang J, Zhu FP,

Yang G, Yan X, Zhang YD, Liu XS. Radiomic analysis of contrast-enhanced CT predicts microvascular invasion and outcome in hepatocellular carcinoma. J Hepatol 2019;70:1133-44.
21. Xv Y, Lv F, Guo H, Liu Z, Luo D, Liu J, Gou X, He W, Xiao M, Zheng Y. A CT-Based Radiomics Nomogram Integrated With Clinic-Radiological Features for Preoperatively Predicting WHO/ISUP Grade of Clear Cell Renal Cell Carcinoma. Front Oncol 2021;11:712554.
22. Alhussaini AJ, Steele JD, Nabi G. Comparative Analysis for the Distinction of Chromophobe Renal Cell Carcinoma from Renal Oncocytoma in Computed Tomography Imaging Using Machine Learning Radiomics Analysis. Cancers (Basel) 2022;14:3609.
23. Tian L, Li Z, Wu K, Dong P, Liu H, Wu S, Zhou F. The clinical significance of computed tomography texture features of renal cell carcinoma in predicting pathological T1-3 staging. Quant Imaging Med Surg 2023;13:2415-25.
24. Zhou Z, Qian X, Hu J, Chen G, Zhang C, Zhu J, Dai Y. An artificial intelligence-assisted diagnosis modeling software (AIMS) platform based on medical images and machine learning: a development and validation study. Quant Imaging Med Surg 2023;13:7504-22.
25. Xv Y, Lv F, Guo H, Zhou X, Tan H, Xiao M, Zheng Y. Machine learning-based CT radiomics approach for predicting WHO/ISUP nuclear grade of clear cell renal cell carcinoma: an exploratory and comparative study. Insights Imaging 2021;12:170.
26. Zheng Z, Chen Z, Xie Y, Zhong Q, Xie W. Development and validation of a CT-based nomogram for preoperative prediction of clear cell renal cell carcinoma grades. Eur Radiol 2021;31:6078-86.
27. Collins GS, Reitsma JB, Altman DG, Moons KG. Transparent reporting of a multivariable prediction model for individual prognosis or diagnosis (TRIPOD): the TRIPOD statement. BMJ 2015;350:g7594.
28. Moons KG, Altman DG, Reitsma JB, Ioannidis JP, Macaskill P, Steyerberg EW, Vickers AJ, Ransohoff DF, Collins GS. Transparent Reporting of a multivariable prediction model for Individual Prognosis or Diagnosis (TRIPOD): explanation and elaboration. Ann Intern Med 2015;162:W1-73.
29. Wei J, Zhao J, Zhang X, Wang D, Zhang W, Wang Z, Zhou J. Analysis of dual energy spectral CT and pathological grading of clear cell renal cell carcinoma (ccRCC). PLoS One 2018;13:e0195699.
30. Kapur P, Zhong H, Araj E, Christie A, Cai Q, Kim D, Miyata J, Tcheuyap VT, Brandenburg O, Carrillo D, Pedrosa I, Brugarolas J, Cadeddu JA. Predicting Oncologic Outcomes in Small Renal Tumors. Eur Urol Oncol 2022;5:687-94.
31. Kuthi L, Jenei A, Hajdu A, Németh I, Varga Z, Bajory Z, Pajor L, Iványi B. Prognostic Factors for Renal Cell Carcinoma Subtypes Diagnosed According to the 2016 WHO Renal Tumor Classification: a Study Involving 928 Patients. Pathol Oncol Res 2017;23:689-98.
32. van Griethuysen JJM, Fedorov A, Parmar C, Hosny A, Aucoin N, Narayan V, Beets-Tan RGH, Fillion-Robin JC, Pieper S, Aerts HJWL. Computational Radiomics System to Decode the Radiographic Phenotype. Cancer Res 2017;77:e104-7.
33. Blagus R, Lusa L. SMOTE for high-dimensional class-imbalanced data. BMC Bioinformatics 2013;14:106.
34. Zwanenburg A, Vallières M, Abdalah MA, Aerts HJWL, Andrearczyk V, Apte A, et al. The Image Biomarker Standardization Initiative: Standardized Quantitative Radiomics for High-Throughput Image-based Phenotyping. Radiology 2020;295:328-38.
35. Lambin P, Leijenaar RTH, Deist TM, Peerlings J, de Jong EEC, van Timmeren J, Sanduleanu S, Larue RTHM, Even AJG, Jochems A, van Wijk Y, Woodruff H, van Soest J, Lustberg T, Roelofs E, van Elmpt W, Dekker A, Mottaghy FM, Wildberger JE, Walsh S. Radiomics: the bridge between medical imaging and personalized medicine. Nat Rev Clin Oncol 2017;14:749-62.
36. Li Q, Liu YJ, Dong D, Bai X, Huang QB, Guo AT, Ye HY, Tian J, Wang HY. Multiparametric MRI Radiomic Model for Preoperative Predicting WHO/ISUP Nuclear Grade of Clear Cell Renal Cell Carcinoma. J Magn Reson Imaging 2020;52:1557-66.
37. Yi X, Xiao Q, Zeng F, Yin H, Li Z, Qian C, Wang C, Lei G, Xu Q, Li C, Li M, Gong G, Zee C, Guan X, Liu L, Chen BT. Computed Tomography Radiomics for Predicting Pathological Grade of Renal Cell Carcinoma. Front Oncol 2020;10:570396.
38. Han D, Yu Y, Yu N, Dang S, Wu H, Jialiang R, He T. Prediction models for clear cell renal cell carcinoma ISUP/WHO grade: comparison between CT radiomics and conventional contrast-enhanced CT. Br J Radiol 2020;93:20200131.
39. He X, Zhang H, Zhang T, Han F, Song B. Predictive models composed by radiomic features extracted from multi-detector computed tomography images for predicting low- and high- grade clear cell renal cell carcinoma: A STARD-compliant article. Medicine (Baltimore) 2019;98:e13957.

40. Li X, Lin J, Qi H, Dai C, Guo Y, Lin D, Zhou J. Radiomics predict the WHO/ISUP nuclear grade and survival in clear cell renal cell carcinoma. Insights Imaging 2024;15:175.
41. Zhou Y, Murugan P, Li F, Bu L. Needle tract seeding in renal tumor biopsies: experience from a single institution. Diagn Pathol 2021;16:43.
42. Bhadauria D, Jose L, Kushwaha R, Kaul A, Nandan R, Singh V, Prasad N. Delayed onset bleed after percutaneous kidney biopsy: is it the same as early bleed? Acta Radiol 2022;63:261-7.
43. Prasad N, Shukla R, Behera M, Yachha M, Bhadauria D, Kaul A, Lal H, Gupta A. Comparison of yield and complications of craniocaudal versus caudocranial needle trajectory for kidney biopsy. J Vasc Access 2020;21:73-8.
44. Motzer RJ, Jonasch E, Agarwal N, Alva A, Baine M, Beckermann K, et al. Kidney Cancer, Version 3.2022, NCCN Clinical Practice Guidelines in Oncology. J Natl Compr Canc Netw 2022;20:71-90.
45. Rathmell WK, Rumble RB, Van Veldhuizen PJ, Al-Ahmadie H, Emamekhoo H, Hauke RJ, Louie AV, Milowsky MI, Molina AM, Rose TL, Siva S, Zaorsky NG, Zhang T, Qamar R, Kungel TM, Lewis B, Singer EA. Management of Metastatic Clear Cell Renal Cell Carcinoma: ASCO Guideline. J Clin Oncol 2022;40:2957-95.

Cite this article as: Xv Y, Wei Z, Lv F, Jiang Q, Guo H, Zheng Y, Zhang X, Xiao M. Multiparameter computed tomography (CT) radiomics signature fusion-based model for the preoperative prediction of clear cell renal cell carcinoma nuclear grade: a multicenter development and external validation study. Quant Imaging Med Surg 2024;14(10):7031-7045. doi: 10.21037/qims-24-35